J. Fluid Mech. (1999), *vol.* 395, *pp.* 61–87. Printed in the United Kingdom

Thermosolutal bifurcation phenomena in porous enclosures subject to vertical temperature and concentration gradients

By M. MAMOU AND P. VASSEUR

Department of Mechanical Engineering, Ecole Polytechnique, University of Montreal, C.P. 6079, Succ. 'Down-Town' Montreal, Quebec, H3C 3A7, Canada
e-mail: vasseur@meca.polymtl.ca

(Received 16 November 1998 and in revised form 14 April 1999)

The Darcy model with the Boussinesq approximations is used to study double-diffusive instability in a horizontal rectangular porous enclosure subject to two sources of buoyancy. The two vertical walls of the cavity are impermeable and adiabatic while Dirichlet or Neumann boundary conditions on temperature and solute are imposed on the horizontal walls. The onset and development of convection are first investigated using the linear and nonlinear perturbation theories. Depending on the governing parameters of the problem, four different regimes are found to exist, namely the stable diffusive, the subcritical convective, the oscillatory and the augmenting direct regimes. The governing parameters are the thermal Rayleigh number, R_T, buoyancy ratio, N, Lewis number, Le, normalized porosity of the porous medium, ε, aspect ratio of the enclosure, A, and the thermal and solutal boundary condition type, κ, applied on the horizontal walls. On the basis of the nonlinear perturbation theory and the parallel flow approximation (for slender or shallow enclosures), analytical solutions are derived to predict the flow behaviour. A finite element numerical method is introduced to solve the full governing equations. The results indicate that steady convection can arise at Rayleigh numbers below the supercritical value, indicating the development of subcritical flows. At the vicinity of the threshold of supercritical convection the nonlinear perturbation theory and the parallel flow approximation results are found to agree well with the numerical solution. In the overstable regime, the existence of multiple solutions, for a given set of the governing parameters, is demonstrated. Also, numerical results indicate the possible occurrence of travelling waves in an infinite horizontal enclosure.

1. Introduction

The analogue of the Rayleigh–Bénard problem in a horizontal porous layer has been much studied in the past. Starting with the early works of Horton & Rogers (1945) and Lapwood (1948), several studies have been conducted to determine the conditions for the onset of motion within porous enclosures subject to various boundary conditions. A wide cross-section of fundamental research on this topic has been reviewed by Cheng (1978) and Nield & Bejan (1999). It is rather surprising that the related problem of the onset and development of convection in porous media saturated with binary mixtures has received marginal attention. The dynamics of heat and mass transfer for flows induced by both temperature and concentration fields, the so-called double-diffusive flows, are however expected to be very different from those

driven by the temperature field solely. Double-diffusive convection in porous media has many applications, among them the migration of moisture in fibrous insulation, contaminant transport in saturated soil, underground disposal of nuclear wastes and electro-chemical and drying processes.

Double-diffusive instability in a horizontal porous layer was first studied by Nield (1968). On the basis of a linear stability analysis, the criterion for the onset of convection was derived for various thermal and solutal boundary conditions. An extension of the analysis was made by Taunton & Lightfoot (1972) to determine the conditions for which 'salt fingers' develop in the presence of both temperature and concentration gradients. The case of sparsely packed porous medium was investigated by Poulikakos (1986) on the basis of the Brinkman-extended Darcy model. The boundaries defining the regions of direct and overstable modes were obtained in terms of the governing parameters of the problem. Malashetty (1993) also relied on linear stability analysis to determine the effect of anisotropic thermo-convective currents and the critical Rayleigh numbers for both marginal and overstable motions.

Rudraiah, Shrimani & Friedrich (1982) applied nonlinear stability analysis to the case of a porous layer with isothermal and isosolutal boundaries. The effects of Prandtl number, ratio of diffusivities and the permeability parameter on finite-amplitude convection were studied. Brand & Steinberg (1983) investigated finite-amplitude convection near the threshold for both stationary and oscillatory instabilities. The temporal behaviour of the Nusselt and Sherwood numbers was predicted for the oscillatory regime. Murray & Chen (1989) investigated experimentally and numerically double-diffusive convection in a horizontal porous layer. In the presence of stabilizing salinity gradients the onset of convection was marked by a dramatic increase in heat flux at a critical temperature difference value. Furthermore, when the temperature difference was reduced to subcritical values the heat flux curve established a hysteresis loop.

A few studies have also been reported concerning the regime of large-amplitude convection within a porous medium subject to vertical gradient of heat and solute. Trevisan & Bejan (1987) investigated the convective mass transfer produced by high thermal Rayleigh number convection in a two-dimensional porous cavity heated isothermally from below. Their numerical results, together with a scale analysis, revealed the existence of different scaling laws for the dependence of the overall mass transfer rate in term of the Lewis number. Natural convection in a porous medium heated from below in a square cavity with two opposing sources of buoyancy (heat and salt) has been studied numerically by Rosenberg & Spera (1992) for a variety of boundary and initial conditions on the salinity field. The effects of the governing parameters on the heat and mass transfer rates were discussed. Double-diffusive fingering convection in a horizontal porous medium, in which horizontally periodic boundary conditions are prescribed, was considered by Chen & Chen (1993). The Darcy equation, including Brinkman and Forchheimer terms, was used for the momentum equation. The stability boundaries which separate regions of different types of convective motion were identified in terms of the thermal and solutal Rayleigh numbers. Mamou *et al.* (1995) considered thermosolutal convection in an inclined porous layer heated and salted from the sides by uniform fluxes of heat and solute. An analytical solution, based on the parallel flow approximation, was found to be in good agreement with the numerical solution of the full governing equations. The possible development of subcritical steady flows, for the case of a horizontal layer, was predicted and confirmed by the numerical results.

The aim of the present analysis is to study double-diffusive convection phenomena in a horizontal porous enclosure subject to vertical gradients of temperature and

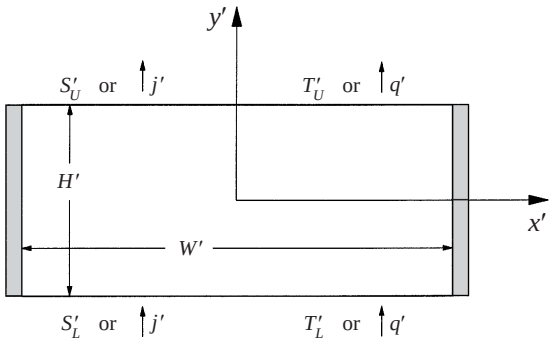

FIGURE 1. Schematic diagram of the physical model and coordinate system.

solute. Analytical solutions are obtained using linear and nonlinear perturbation theories and the parallel flow approximation. The results are verified numerically by solving the full nonlinear set of governing equations with a finite element method.

The content of the present work is organized as follows. In the next section (§ 2) the physical system is described and a mathematical model of the problem is derived. In § 3, the finite element numerical model used for solving the full governing equations is discussed. In § 4, two nonlinear theories are proposed to study the bifurcation character near the threshold of monotonic convection: the first one is based on the nonlinear perturbation theory and the second one on the parallel flow approximation for slender or shallow enclosures. Finally, in § 5, some relevant conclusions about the present findings are stated.

2. Mathematical formulation

The physical model considered in the present study is a two-dimensional horizontal porous layer of height H' and width W' (see figure 1). The two vertical walls of the cell are assumed impermeable and adiabatic while Dirichlet or Neumann boundary conditions are applied, for both temperature and concentration, on the horizontal walls. The convective motion in the homogeneous isotropic porous medium is assumed to be governed by the Darcy law for which inertia and viscous effects are negligible. The interaction between heat and mass transfer, known as Soret and Dufour effects, are supposed to have no influence on the convective flow (see, for instance, De Groot & Mazur 1962 and Bergman & Shrinivasan 1989), so they are neglected. The binary mixture that saturates the porous matrix is modelled as a Newtonian Boussinesq incompressible fluid whose density, ρ, varies linearly with temperature, T', and solute concentration, S', as

$$\rho = \rho_0[1 - \beta_T(T' - T'_0) - \beta_S(S' - S'_0)], \tag{2.1}$$

where ρ_0 is the density at temperature $T' = T'_0$ and solute concentration $S' = S'_0$, β_T and β_S are the thermal and solutal expansion coefficients, respectively and 0 denotes a reference state.

The dimensionless equations describing conservation of momentum, energy and solute in the solution-saturated porous medium are respectively

$$\nabla^2 \Psi = -\left(R_T \frac{\partial T}{\partial x} + \frac{R_S}{Le}\frac{\partial S}{\partial x}\right), \tag{2.2}$$

$$\frac{\partial T}{\partial t} - \mathcal{J}(\Psi, T) = \nabla^2 T, \tag{2.3}$$

$$\varepsilon \frac{\partial S}{\partial t} - \mathcal{J}(\Psi, S) = \frac{1}{Le} \nabla^2 S, \tag{2.4}$$

where $\mathcal{J}$ is the usual Jacobian operator,

$$\mathcal{J}(f, g) = \frac{\partial f}{\partial x}\frac{\partial g}{\partial y} - \frac{\partial f}{\partial y}\frac{\partial g}{\partial x},$$

and Ψ is the stream function defined as

$$u = \frac{\partial \Psi}{\partial y}, \qquad v = -\frac{\partial \Psi}{\partial x} \tag{2.5}$$

such that the mass conservation is satisfied.

The above equations were non-dimensionalized with the use of the following scales:

$$\left.\begin{aligned} (x, y) &= \left(\frac{x'}{\ell^*}, \frac{y'}{\ell^*}\right), \quad t = \frac{t'\alpha}{\sigma \ell^{*2}}, \quad (u, v) = \left(\frac{u'\ell^*}{\alpha}, \frac{v'\ell^*}{\alpha}\right), \\ \Psi &= \frac{\Psi'}{\alpha}, \quad S = \frac{(S' - S'_0)}{\Delta S^*}, \quad T = \frac{(T' - T'_0)}{\Delta T^*}, \end{aligned}\right\} \tag{2.6}$$

where u' and v' are the volume-averaged velocity components, t' is the time, α and σ are thermal diffusivity of the saturated porous medium and saturated porous medium to fluid heat capacity ratio, respectively. The length scale, ℓ^*, is set to H' when $A \geqslant 1$ and to W' when $A < 1$. Here, A is the aspect ratio of the enclosure defined as $A = W'/H'$.

The definitions of T'_0, S'_0, ΔT^* and ΔS^* are related to the thermal and solutal boundary conditions. They are given by

$$\left.\begin{aligned} T'_0 &= \kappa\, T'_{(0,0)} + (1-\kappa)\frac{T'_L + T'_U}{2}, \quad S'_0 = \kappa\, S'_{(0,0)} + (1-\kappa)\frac{S'_L + S'_U}{2}, \\ \Delta T^* &= \kappa\, \frac{q'H'}{k} + (1-\kappa)(T'_L - T'_U), \quad \Delta S^* = \kappa\, \frac{j'H'}{D} + (1-\kappa)(S'_L - S'_U), \end{aligned}\right\} \tag{2.7}$$

where the subscript $(0,0)$ denotes the origin of the coordinates system, the subscripts L and U refer to the lower and the upper horizontal boundaries respectively, D is the mass-averaged diffusivity through the fluid-saturated porous medium, k the thermal conductivity of the saturated porous medium and the quantities q' and j' are the constant fluxes of heat and mass (per unit area) applied on the horizontal walls. The parameter κ is set equal to zero for Dirichlet boundary conditions and to 1 for Neumann ones.

The dimensionless boundary conditions depicted in figure 1 are expressed by

$$x = \pm \frac{A_x}{2}, \quad \Psi = 0 \quad \text{and} \quad \frac{\partial \varphi}{\partial x} = 0, \tag{2.8}$$

$$y = \pm \frac{A_y}{2}, \quad \Psi = 0 \quad \text{and} \quad \kappa\, A_y \frac{\partial \varphi}{\partial y} \pm (1-\kappa)\varphi = -\frac{\kappa + 1}{2}, \tag{2.9}$$

where φ stands for T and S, A_x and A_y are the aspect ratio of the enclosure in the x- and y-directions, respectively, defined by

$$\left.\begin{aligned} &A_x = A \quad \text{and} \quad A_y = 1 \quad \text{for} \quad A \geqslant 1, \\ &A_x = 1 \quad \text{and} \quad A_y = 1/A \quad \text{for} \quad A < 1. \end{aligned}\right\} \tag{2.10}$$

The dimensionless parameters governing the present problem are the thermal Rayleigh number, R_T, the solutal Rayleigh number, R_S, the Lewis number, Le, the aspect ratio of the cavity, A, and the normalized porosity of the porous medium, ε. They are defined respectively by

$$R_T = \frac{g\ \beta_T\ K\ \Delta T^*\ \ell^*}{\alpha \nu}, \quad R_S = \frac{g\ \beta_S\ K\ \Delta S^*\ \ell^*}{D\nu}, \quad Le = \frac{\alpha}{D}, \quad A = \frac{W'}{H'}, \quad \varepsilon = \frac{\epsilon}{\sigma}, \tag{2.11}$$

where K is the permeability of the porous medium, g the acceleration due to gravity, ν the kinematic viscosity of the fluid and ϵ the porosity of the porous medium.

It is noted that the volumetric expansion coefficient, β_T, due to temperature fluctuation is usually positive, but that due to solute concentration variation, β_S, can be either positive or negative. Thus, with the thermal and solutal boundary conditions considered here, heat destabilizes the vertical density gradient while salt is destabilizing for $\beta_S > 0$ and stabilizing for $\beta_S < 0$.

At this stage, since we are interested in investigating the stability of the system under study, it is convenient to consider the pure diffusive solution as a part of the total one. Thus we introduce the following transformations:

$$\left.\begin{aligned} \Psi(t,x,y) &= \Psi_C + \psi(t,x,y), \\ T(t,x,y) &= T_C + \theta(t,x,y), \\ S(t,x,y) &= S_C + \phi(t,x,y), \end{aligned}\right\} \tag{2.12}$$

where (Ψ_C, T_C, S_C) is the static state of the system described by

$$\Psi_C = 0, \quad T_C = -\frac{y}{A_y}, \quad S_C = -\frac{y}{A_y}, \tag{2.13}$$

and $\psi(t,x,y)$, $\theta(t,x,y)$ and $\phi(t,x,y)$ are the deviations from the rest-state solution resulting from the convective effects.

Upon substituting (2.12) and (2.13) into (2.2)–(2.4), the resulting governing equations expressing conservation of momentum, energy and solute reduce to

$$\left.\begin{aligned} \nabla^2\psi &= -\left(R_T\frac{\partial\theta}{\partial x} + \frac{R_S}{Le}\frac{\partial\phi}{\partial x}\right), \\ \frac{\partial\theta}{\partial t} + \frac{1}{A_y}\frac{\partial\psi}{\partial x} - \mathcal{J}(\psi,\theta) &= \nabla^2\theta, \\ \varepsilon\frac{\partial\phi}{\partial t} + \frac{1}{A_y}\frac{\partial\psi}{\partial x} - \mathcal{J}(\psi,\phi) &= \frac{1}{Le}\ \nabla^2\phi, \end{aligned}\right\} \tag{2.14}$$

respectively and the boundary conditions to

$$\left.\begin{aligned} x = \pm\frac{A_x}{2}, \quad \psi = 0, \quad \frac{\partial\varphi}{\partial x} = 0, \\ y = \pm\frac{A_y}{2}, \quad \psi = 0, \quad \kappa\ \frac{\partial\varphi}{\partial y} + (1-\kappa)\ \varphi\ = 0. \end{aligned}\right\} \tag{2.15}$$

According to the thermal and solutal boundary conditions applied on the horizontal walls of the cavity, the local heat and mass transfer rates are expressed in terms of

the Nusselt and Sherwood numbers as

$$\left.\begin{aligned} Nu &= \kappa\,\frac{1}{T_{(x,-A_y/2)}-T_{(x,A_y/2)}} - (1-\kappa)\frac{\partial T}{\partial y}\bigg|_{y=\pm A_y/2}, \\ Sh &= \kappa\,\frac{1}{S_{(x,-A_y/2)}-S_{(x,A_y/2)}} - (1-\kappa)\frac{\partial S}{\partial y}\bigg|_{y=\pm A_y/2}. \end{aligned}\right\} \tag{2.16}$$

The corresponding mean values along the horizontal walls can be computed from the following integrals:

$$\overline{Nu} = \frac{1}{A_x}\int_{-A_x/2}^{A_x/2} Nu\,\mathrm{d}y, \qquad \overline{Sh} = \frac{1}{A_x}\int_{-A_x/2}^{A_x/2} Sh\,\mathrm{d}y. \tag{2.17}$$

3. Numerical solution

A finite element method is used to solve the governing equations (2.14) with the boundary conditions (2.15). Since the details of the present numerical procedure are discussed by Mamou, Vasseur & Bilgen (1998*a*) only the main steps are presented here. The calculus domain is discretized into rectangular elements known as the nine-noded Lagrangian cubic elements, with uniform grids. The temporal derivatives in the energy and solute concentration equations are discretized according to the finite difference scheme. First- (for the first time step) and second-order backward schemes are used. The governing equations are discretized using the Bubnov–Galerkin procedure with an implicit scheme. The resulting discretized momentum equation is solved by the successive over relaxation method (SOR). The energy and concentration equations are solved by an iterative procedure based on the pentadiagonal matrix algorithm (PDMA). Depending on the governing parameters values, the grid size was varied from 20×20 to 20×50 and the time step, Δt, from 10^{-4} to 10^{-3}.

The computer code has been validated for various cases and the results are published elsewhere (Mamou *et al.* 1995; Mamou 1998). The comparison of our results with those available in the literature indicates that, in general, the maximum deviation is less than about 0.5%.

4. Analytical solution

In this section we study the onset and development of convection within a porous rectangular cavity using the nonlinear perturbation theory. First, finite-amplitude convection is investigated on the basis of a truncated representation of Fourier series. The resulting nonlinear equations are solved on the assumption that the motion is steady. Then the linear theory is used to predict the thresholds of both marginal and overstable motions. Finally, an analytical solution, based on the parallel flow approximation, is derived for the special case of a shallow ($A \gg 1$) or slender ($A \ll 1$) enclosure subject to Neumann boundary conditions.

4.1. *Nonlinear perturbation theory*

Finite-amplitude convection in a porous cavity saturated with a binary fluid is now investigated using a limited representation of Fourier series. Analytical solutions will be derived for the cases of Dirichlet and Neumann boundary conditions. In general, it was demonstrated by Veronis (1968), Platten & Legros (1984) and Ahlers & Lücke

(1987) that, at the vicinity of the onset of convection, the perturbation profiles can be approximated by the following relations:

$$\left.\begin{aligned} \psi(t,x,y) &= \psi_0(t)\ F(x,y), \\ \theta(t,x,y) &= \theta_0(t)\ G(x,y) + \theta_1(t)\ h(x,y), \\ \phi(t,x,y) &= \phi_0(t)\ G(x,y) + \phi_1(t)\ h(x,y), \end{aligned}\right\} \tag{4.1}$$

where the amplitude ψ_0, θ_0, θ_1, ϕ_0 et ϕ_1 are time functions while $F(x,y)$, $G(x,y)$ and $h(x,y)$ are space functions describing the perturbation profiles at the vicinity of the onset of convection. These functions satisfy the boundary conditions given by (2.15). According to Veronis (1968), Platten & Legros (1984) and Ahlers & Lücke (1987), the functions $F(x,y)$ and $G(x,y)$ can be chosen as the temperature and concentration perturbation profiles corresponding to the onset of monotonic convection and the function $h(x,y)$ as

$$\left.\begin{aligned} h(x,y) &= \sin(2r_y y) \quad \text{when } \kappa = 0, \\ h(x,y) &= \sin(r_y y) \quad \text{when } \kappa = 1, \end{aligned}\right\} \tag{4.2}$$

where $r_y = \pi/A_y$.

Substituting (4.1) into (2.14), using $F(x,y)$, $G(x,y)$ and $h(x,y)$ as the weighted functions and the Green theorem, the weak Galerkin formulation leads to the following set of ordinary differential equations:

$$\mathscr{K}_\psi\ \psi_0 = \mathscr{B}\left(R_T\theta_0 + \frac{R_S}{Le}\phi_0\right), \tag{4.3}$$

$$\left.\begin{aligned} \mathscr{M}\frac{\mathrm{d}\theta_0}{\mathrm{d}t} - \frac{\mathscr{L}}{A_y}\psi_0 + \mathscr{L}_1\psi_0\theta_1 &= -\mathscr{K}\ \theta_0, \\ \mathscr{M}_1\frac{\mathrm{d}\theta_1}{\mathrm{d}t} - \mathscr{L}_2\psi_0\theta_0 &= -\mathscr{K}_1\ \theta_1, \end{aligned}\right\} \tag{4.4}$$

$$\left.\begin{aligned} \varepsilon\mathscr{M}\frac{\mathrm{d}\phi_0}{\mathrm{d}t} - \frac{\mathscr{L}}{A_y}\psi_0 + \mathscr{L}_1\psi_0\phi_1 &= -\frac{\mathscr{K}}{Le}\ \phi_0, \\ \varepsilon\mathscr{M}_1\frac{\mathrm{d}\phi_1}{\mathrm{d}t} - \mathscr{L}_2\psi_0\phi_0 &= -\frac{\mathscr{K}_1}{Le}\ \phi_1, \end{aligned}\right\} \tag{4.5}$$

where the constants $\mathscr{B}$, $\mathscr{K}_\psi$, $\mathscr{K}$, $\mathscr{L}$, $\mathscr{L}_1$, $\mathscr{L}_2$, $\mathscr{M}$ and $\mathscr{M}_1$ can be evaluated from the integrals

$$\left.\begin{aligned} \mathscr{B} &= \int_\Omega \frac{\partial G}{\partial x}F\ \mathrm{d}\Omega, \quad \mathscr{K} = \int_\Omega (\nabla G)^2\ \mathrm{d}\Omega, \quad \mathscr{K}_\psi = \int_\Omega (\nabla F)^2 \mathrm{d}\Omega, \\ \mathscr{K}_1 &= \int_\Omega (\nabla h)^2\ \mathrm{d}\Omega, \quad \mathscr{L} = \int_\Omega \frac{\partial F}{\partial x}G\ \mathrm{d}\Omega, \quad \mathscr{M} = \int_\Omega G^2\ \mathrm{d}\Omega, \\ \mathscr{M}_1 &= \int_\Omega h^2\ \mathrm{d}\Omega, \quad \mathscr{L}_1 = -\int_\Omega \mathscr{J}(F,h)G\ \mathrm{d}\Omega, \quad \mathscr{L}_2 = \int_\Omega \mathscr{J}(F,G)h\ \mathrm{d}\Omega, \end{aligned}\right\} \tag{4.6}$$

Ω being the physical domain of integration. Below, these integrals will be performed for the cases of Dirichlet and Neumann boundary conditions respectively.

(i) *Constant temperatures and concentrations* ($\kappa = 0$)

This situation corresponds to the Bénard problem for which the exact analytical

profiles of the functions $F(x, y)$ and $G(x, y)$ are given by

$$F(x, y) = f(x)\cos(r_y y), \qquad G(x, y) = g(x)\cos(r_y y), \tag{4.7}$$

where $r_y = \pi/A_y$ and the functions $f(x)$ and $g(x)$ are defined as

$$\left.\begin{aligned} f(x) &= \cos(r_x x) \ \text{ and } \ g(x) = \sin(r_x x) \ \text{ for } \ n = 1, 3, \ldots, \\ f(x) &= \sin(r_x x) \ \text{ and } \ g(x) = \cos(r_x x) \ \text{ for } \ n = 2, 4, \ldots, \end{aligned}\right\} \tag{4.8}$$

where $r_x = n\pi/A_x$ and n is the number of cells.

Substituting (4.2) and (4.7) into (4.6) and performing the resulting integrals, it is readily found that

$$\left.\begin{aligned} \mathscr{B} &= -(-1)^n r_x \mathscr{D}, \quad \mathscr{K} = (r_x^2 + r_y^2)\mathscr{D}, \quad \mathscr{K}_\psi = (r_x^2 + r_y^2)\mathscr{D}, \\ \mathscr{K}_1 &= 8r_y^2 \mathscr{D}, \quad \mathscr{L} = -(-1)^n r_x \mathscr{D}, \quad \mathscr{L}_1 = (-1)^n r_x r_y \mathscr{D}, \\ \mathscr{L}_2 &= (-1)^n r_x r_y \mathscr{D}, \quad \mathscr{M} = \mathscr{D}, \quad \mathscr{M}_1 = 2\mathscr{D}, \end{aligned}\right\} \tag{4.9}$$

where $\mathscr{D} = A_x A_y/4$.

(ii) *Constant fluxes of heat and solute* ($\kappa = 1$)

When the horizontal walls are subject to constant fluxes of heat and solute, it can be demonstrated easily that $F(x, y)$ and $G(x, y)$ have the expressions

$$\left.\begin{aligned} F(x, y) &= \cos(r_x x)[\cosh(\xi_0 y) - \gamma_0 \cos(\eta_0 y)], \\ G(x, y) &= \sin(r_x x)[\cosh(\xi_0 y) + \gamma_0 \cos(\eta_0 y)], \end{aligned}\right\} \tag{4.10}$$

where γ_0, ξ_0, η_0 and r_x are defined as

$$\left.\begin{aligned} \xi_0 &= \sqrt{r_x(\sqrt{R_0^{sup}} + r_x)}, \quad \eta_0 = \sqrt{r_x(\sqrt{R_0^{sup}} - r_x)}, \\ \gamma_0 &= \frac{\cosh(\xi_0 A_y/2)}{\cos(\eta_0 A_y/2)}, \quad r_x = \frac{\pi}{A_x}, \end{aligned}\right\} \tag{4.11}$$

and R_0^{sup} is a constant which can be computed from the relation

$$\xi_0 \ \tanh(\xi_0 A_y/2) \ = \ \eta_0 \ \tan(\eta_0 A_y/2). \tag{4.12}$$

For this case, (4.6) together with (4.2) and (4.10) yields

$$\left.\begin{aligned} \mathscr{B} &= \pi(a_1 - \gamma_0^2 a_3)/2, \quad \mathscr{K} = \pi\sqrt{R_0^{sup}}(a_1 - \gamma_0^2 a_3)/2, \\ \mathscr{K}_\psi &= \pi\sqrt{R_0^{sup}}(a_1 - \gamma_0^2 a_3)/2, \quad \mathscr{K}_1 = \pi^2(A_x/2), \\ \mathscr{L} &= \pi(a_1 - \gamma_0^2 a_3)/2, \quad \mathscr{M} = (a_1 + 2\gamma_0 a_2 + \gamma_0^2 a_3)(A_x/2), \\ \mathscr{M}_1 &= A_x/2, \quad \mathscr{L}_1 = \pi^2(a_4 - \gamma_0^2 a_5)/2, \\ \mathscr{L}_2 &= \frac{\pi}{2}\left(\frac{4\xi_0^2}{4\xi_0^2 + r_y^2}\cosh(\xi_0 A_y) - \gamma_0^2 \frac{4\eta_0^2}{4\eta_0^2 - r_y^2}\cos(\eta_0 A_y)\right), \end{aligned}\right\} \tag{4.13}$$

where

$$\left.\begin{aligned} a_1 &= \frac{1}{2}\left(A_y + \frac{\sinh(\xi_0 A_y)}{\xi_0}\right), \quad a_2 = \frac{4\xi_0}{\xi_0^2+\eta_0^2}\sinh(\xi_0 A_y/2)\cos(\eta_0 A_y/2), \\ a_3 &= \frac{1}{2}\left(A_y + \frac{\sin(\eta_0 A_y)}{\eta_0}\right), \quad a_4 = \frac{A_y}{\pi} + \frac{r_y}{4\xi_0^2+r_y^2}\cosh(\eta_0 A_y), \\ a_5 &= \frac{A_y}{\pi} - \frac{r_y}{4\eta_0^2-r_y^2}\cos(\eta_0 A_y). \end{aligned}\right\} \quad (4.14)$$

4.1.1. *Linear analysis*

The stability of the rest state of the system ($\Psi_C = 0$, $T_C = S_C = -y/A_y$) is predicted upon assuming that amplitudes $\psi_0(t)$, $\theta_0(t)$, $\theta_1(t)$, $\phi_0(t)$ and $\phi_1(t)$, in (4.3)–(4.5), are small enough and can be expressed as

$$\psi_0(t) = \psi_0 e^{pt}, \quad \theta_0(t) = \theta_0 e^{pt}, \quad \theta_1(t) = \theta_1 e^{pt}, \quad \phi_0(t) = \phi_0 e^{pt}, \quad \phi_1(t) = \phi_1 e^{pt}, \quad (4.15)$$

where p is the growth rate of the perturbation amplitude. Infinitesimal perturbations of the rest state may either damp or grow depending on the value of the parameter p.

Substituting (4.15) into (4.3)–(4.5), neglecting the small nonlinear terms and after some algebra, we readily arrive at the dispersion relationship

$$\varepsilon^2\, Le^2\, p^2 - \gamma\, \varepsilon\, Le\, p_1\, p - \gamma^2 p_2 = 0, \quad (4.16)$$

where

$$p_1 = \varepsilon Le(R_T^0 - 1) + R_S^0 - 1, \qquad p_2 = \varepsilon Le(R_T^0 + R_S^0 - 1), \quad (4.17)$$

and

$$R_T^0 = \frac{R_T}{R_0^{sup}}, \qquad R_S^0 = \frac{R_S}{R_0^{sup}}, \qquad R_0^{sup} = A_y\, R^{sup}, \quad (4.18)$$

in which

$$R^{sup} = \frac{\mathscr{K}_\psi \mathscr{K}}{\mathscr{B}\mathscr{L}}, \qquad \gamma = \frac{\mathscr{K}}{\mathscr{M}}. \quad (4.19)$$

In the above equations, the parameter R_0^{sup} depends only on the aspect ratio of the enclosure, A, and on the thermal and solutal boundary conditions types, κ. When $\kappa = 0$, it can de demonstrated from (4.9), (4.18) and (4.19) that the value of this parameter is given by $R_0^{sup} = A_y(r_x^2 + r_y^2)^2/r_x^2$. However, when $\kappa = 1$, R_0^{sup} has to be determined by solving numerically (4.12) using, for instance, the Newton–Raphson procedure. From a physical point of view the parameter R_0^{sup} corresponds to the supercritical Rayleigh number for the onset of convection in a system destabilized solely by a thermal gradient (i.e. Rayleigh–Bénard convection, $R_S = N = 0$).

Solving (4.16) for p, it is readily found that

$$p = \frac{\gamma}{2\varepsilon Le}\left(p_1 \pm \sqrt{p_1^2 + 4p_2}\right), \quad (4.20)$$

where, in general, the constant p is a complex number which can be decomposed as $p = p_r + ip_i$, where p_r and p_i are the real and imaginary parts respectively. From (4.20)

it is observed that

$$\left.\begin{array}{l} \left.\begin{array}{l} p_r = \dfrac{\gamma}{2\varepsilon Le}\left(p_1 \pm \sqrt{p_1^2 + 4p_2}\right) \\ p_i = 0 \end{array}\right\} \text{ if } p_1^2 + 4p_2 \geqslant 0, \\ \left.\begin{array}{l} p_r = \dfrac{\gamma}{2\varepsilon Le} p_1 \\ p_i = \pm\dfrac{\gamma}{2\varepsilon Le}\sqrt{|p_1^2 + 4p_2|} \end{array}\right\} \text{ if } p_1^2 + 4p_2 < 0. \end{array}\right\} \tag{4.21}$$

The marginal state of instability corresponds to $p = 0$ from which the supercritical Rayleigh number for the onset of supercritical convection, R_{TC}^{sup}, is given by

$$R_{TC}^{sup} = (1 - R_S^0)R_0^{sup} \quad \text{or} \quad R_{TC}^{sup} = \frac{R_0^{sup}}{1 + NLe}, \tag{4.22}$$

where the subscript C refers to a critical state and N is the solutal to thermal buoyancy ratio defined as

$$N = \frac{\beta_S \Delta S^*}{\beta_T \Delta T^*} = \frac{R_S}{Le R_T}. \tag{4.23}$$

The marginal state of instability at which oscillatory convection may arise, corresponds to $p_r = 0$ and $p_i \neq 0$, i.e. $p_1 = 0$. From (4.17) it follows that the overstable critical Rayleigh number, R_{TC}^{over}, for the onset of oscillatory flow, when expressed in terms of R_S or N, is given by

$$R_{TC}^{over} = \frac{(\varepsilon Le + 1 - R_S^0)}{\varepsilon Le} R_0^{sup} \quad \text{or} \quad R_{TC}^{over} = \frac{(\varepsilon Le + 1)}{Le(\varepsilon + N)} R_0^{sup}. \tag{4.24}$$

The oscillatory convective regime ($p_r \geqslant 0$ and $p_i \neq 0$) is expected to exist up to a critical Rayleigh number R_{TC}^{osc} at which the transition from the oscillatory to the direct mode occurs. Thus, overstability exists only when the conditions $p_1^2 + 4p_2 < 0$ and $p_1 > 0$ are satisfied, i.e. $R_{TC}^{over} \leqslant R_T \leqslant R_{TC}^{osc}$ where the value of R_{TC}^{osc} is deduced from the condition $p_1^2 + 4p_2 = 0$ as

$$R_{TC}^{osc} = \frac{\left(\sqrt{\varepsilon Le - 1} + \sqrt{-R_S^0}\right)^2}{\varepsilon Le} R_0^{sup} \quad \text{or} \quad R_{TC}^{osc} = \frac{(\varepsilon Le - 1)}{Le(\sqrt{\varepsilon} - \sqrt{-N})^2} R_0^{sup}. \tag{4.25}$$

On an (R_T, R_S)-plane, the three critical Rayleigh numbers (R_{TC}^{over}, R_{TC}^{osc} and R_{TC}^{sup}) intersect at a point Q having the coordinates

$$(R_T, R_S) = \left(\frac{\varepsilon Le}{\varepsilon Le - 1} R_0^{sup}, \frac{-1}{\varepsilon Le - 1} R_0^{sup}\right). \tag{4.26}$$

From (4.25) and (4.26), it is clear that the oscillatory regime exists only when $R_S < 0$ ($N < 0$) and more specifically when

$$\left.\begin{array}{l} R_T^0 > \dfrac{\varepsilon Le}{\varepsilon Le - 1}, \qquad Le > \dfrac{1}{\varepsilon}, \\ \text{or} \\ R_S^0 < -\dfrac{1}{(\varepsilon Le - 1)}, \qquad \dfrac{1}{\varepsilon Le^2} < -N < \dfrac{1}{Le}. \end{array}\right\} \tag{4.27}$$

4.1.2. *Nonlinear analysis*

The linear stability theory describes only the size of the convective cells and the time evolution of small-amplitude flows. For finite-amplitude convection, a nonlinear theory is required.

Assuming that the flow is steady, it is readily found from (4.4) and (4.5) that

$$\theta_0 = \frac{\mathscr{L}\ \psi_0/A_y}{\mathscr{K} + \dfrac{\mathscr{L}_2\mathscr{L}_1}{\mathscr{K}_1}\ \psi_0^2}, \qquad \phi_0 = \frac{\mathscr{L}Le\ \psi_0/A_y}{\mathscr{K} + \dfrac{\mathscr{L}_2\mathscr{L}_1}{\mathscr{K}_1}Le^2\ \psi_0^2}. \tag{4.28}$$

Substituting the above results into (4.3) yields, after some algebraic simplifications, the following equation for the amplitude ψ_0:

$$\psi_0(Le^4\psi_0^4 - 2aLe^2d_1\psi_0^2 - a^2d_2) = 0, \tag{4.29}$$

where

$$d_1 = Le^2(R_T^0 - 1) + R_S^0 - 1, \quad d_2 = 4Le^2(R_T^0 + R_S^0 - 1), \quad a = \frac{\mathscr{K}\mathscr{K}_1}{2\mathscr{L}_1\mathscr{L}_2}, \tag{4.30}$$

where R_T^0 and R_S^0 are defined in (4.18)

The possible solutions of equation (4.29) are

$$\psi_0 = 0 \tag{4.31}$$

and

$$\psi_0 = \pm\frac{\sqrt{a}}{Le}\left(d_1 \pm \sqrt{d_1^2 + d_2}\right)^{1/2}. \tag{4.32}$$

According to the above results, five different steady-state solutions are possible. One corresponds to the pure diffusive regime ($\psi_0 = 0$) and the others to convective regimes. In (4.32) the plus or minus sign in front of the right-hand side expression indicates that the direction of the fluid circulation can be either clockwise or counterclockwise. On the other hand, the plus or minus sign within the brackets indicates that two different convective solutions are possible.

From a mathematical point of view, (4.32) shows that, depending on the governing parameters values, the primary steady bifurcation can be supercritical or subcritical. When the bifurcation is supercritical a stable branch of solutions, corresponding to supercritical convection, is initiated at a supercritical Rayleigh number, R_{TC}^{sup}, with zero amplitude at the threshold as will be discussed later. When the bifurcation is subcritical two branches of solutions appear, one stable and the other unstable. These two branches are connected to each other at a saddle-node point $R_T = R_{TC}^{sub}$ corresponding to the subcritical Rayleigh number for the onset of finite-amplitude convection.

Supercritical bifurcation occurs, in general, for additive flows ($R_S > 0$) and for opposing flows ($R_S < 0$) when $Le < 1$. For this situation, the supercritical Rayleigh number, R_{TC}^{sup}, corresponding to the onset of supercritical motion is obtained from the conditions $d_1 < 0$ and $d_2 = 0$ (i.e. $\psi_0 = 0$) as

$$R_{TC}^{sup} = (1 - R_S^0)R_0^{sup} \quad \text{or} \quad R_{TC}^{sup} = \frac{R_0^{sup}}{1 + NLe}, \tag{4.33}$$

which is the same result as that predicted by the linear stability analysis, (4.22).

On the other hand, subcritical bifurcation is possible only for the case of opposing flows ($R_S < 0$) when $Le > 1$. At the saddle-node point, the flow intensity is finite

and the subcritical Rayleigh number, R_{TC}^{sub}, for the onset of subcritical convection is obtained, from the conditions $d_1 > 0$ and $d_1^2 + d_2 = 0$, as

$$R_{TC}^{sub} = Le^{-2}\left(\sqrt{Le^2-1}+\sqrt{-R_S^0}\right)^2 R_0^{sup} \quad \text{or} \quad R_{TC}^{sub} = \frac{Le^2-1}{Le(\sqrt{Le}-\sqrt{-N})^2}R_0^{sup}. \tag{4.34}$$

At the threshold R_{TC}^{sub}, the flow intensity is given by

$$\psi_0 = \pm\frac{\sqrt{ad_1}}{Le}. \tag{4.35}$$

The present solution indicates that the occurrence of subcritical convection is related not only to N or R_S but also to Le. Thus, it can be easily demonstrated that the conditions

$$R_S < 0, \qquad Le > \sqrt{(R_S^0-1)/R_S^0} \tag{4.36}$$

or

$$N < 0, \qquad Le > \max\left(-N, \frac{1}{(-N)^{1/3}}\right) \tag{4.37}$$

must be satisfied for the existence of subcritical convection.

4.1.3. *Results and discussion*

The influence of the aspect ratio, A, of the cavity on the critical number R^{sup} is presented in figure 2(a). For a square cavity, $A = 1$, it is well known that the flow pattern consists of a single convective cell and that $R^{sup} = 4\pi^2$ when $\kappa = 0$ (Nield 1968) and $R^{sup} = 22.946$ when $\kappa = 1$ (Kimura, Vynnycky & Alavyoon 1995). For $A < 1$ the only flow configuration possible, independently of the values of A and κ, is a single cell. As a result, the critical number R^{sup} decreases monotonically towards π^2 as the value of A approaches 0. This limit was predicted by Vasseur, Satish & Robillard (1987) for the case $\kappa = 1$. On the other hand, upon increasing A above unity, the results are observed to depend strongly on κ. For $\kappa = 1$, the flow remains unicellular and the value of R^{sup} decreases monotonically with A towards the value 12 predicted by Nield (1968). However, when $\kappa = 0$, as it is well known, the flow can be monocellular or multicellular depending on the aspect ratio of the cavity. Thus, upon increasing A from 1 up to $\sqrt{2}$, a one-cell mode prevails and R^{sup} increases from $4\pi^2$ to $9\pi^2/2$. At $A = \sqrt{2}$, two solutions are possible: one corresponds to a monocellular flow and the other to a bicellular flow. The two flow configurations have the same critical number, R^{sup}. Above $A = \sqrt{2}$, the flow exhibits a two-cell mode and R^{sup} decreases from $9\pi^2/2$ to $4\pi^2$ as the value of A reaches 2. This process continues as the value of A is made larger, the value $R^{sup} = 4\pi^2$ being reached for all integer values of A. All the peaks in figure 2(a) denote a transition between two different convective modes.

Figure 2(b) illustrates the variation of the parameter γ, (4.19), as function of the aspect ratio, A, of the enclosure. According to (4.20), the perturbation amplitude growth parameter p is a linear function of γ. The increase of γ results in increasing the absolute values of p_r and p_i. In other words, the variation rate of the amplitude perturbation and the oscillation frequency increase with increasing γ. For $A \leqslant 1$, the parameter γ is seen to tend towards the asymptotic value π^2 when A is made small enough. For $A \geqslant 1$ and $\kappa = 1$, γ is observed to decrease towards zero when A is made large enough. Thus, for large aspect ratio the amplitude perturbation growth rate becomes very small and it takes a considerable time to give rise to a convective flow.

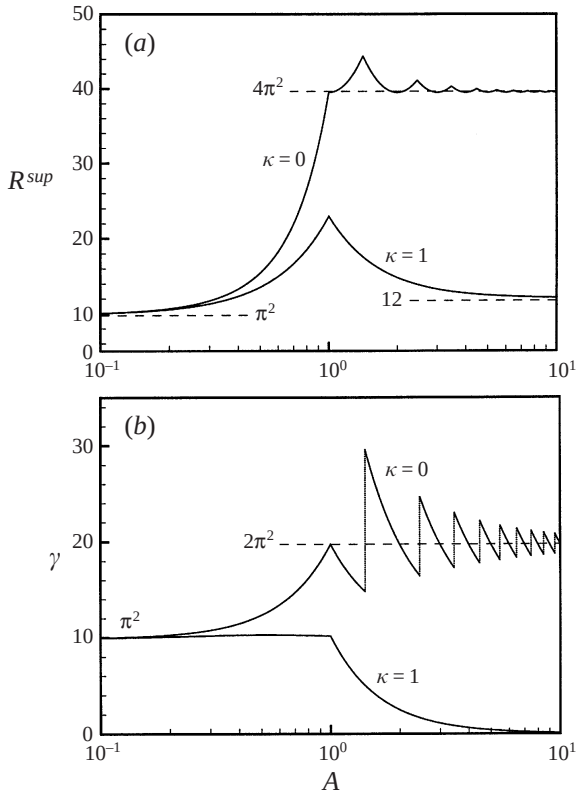

FIGURE 2. (*a*) Parameter R^{sup} and (*b*) parameter γ as a function of the aspect ratio A for $\kappa = 0$ and 1.

However, for $\kappa = 0$, as shown in figure 2(*b*), γ undergoes an irregular variation with A and tends asymptotically towards the constant $2\pi^2$ as the value of A is made large enough. The jumps in figure 2(*b*) correspond to transitions from a n to a $(n+1)$ cells flow structure.

In figures 3(*a*) and 3(*b*) the thermal and solutal Rayleigh numbers, R_T and R_S, are normalized with respect to the constant R_0^{sup}, (4.18). Also, the amplitude ψ_0 of the stream function is normalized with respect to $\sqrt{a}$ (i.e. $\psi_a = \psi_0/\sqrt{a}$). The results presented in these graphs are thus independent of the aspect ratio A of the cavity and the thermal and solutal boundary conditions types, κ.

Figure 3(*a*) shows the stability diagram for $Le = 10$ and $\varepsilon = 0.2$ in which four regions are delineated by the curves corresponding to R_{TC}^{sub}, R_{TC}^{over}, R_{TC}^{osc} and R_{TC}^{sup} as given by (4.34), (4.24), (4.25) and (4.33), respectively. In region I, below the subcritical Rayleigh number R_{TC}^{sub}, the fluid is expected to remain stable according to both linear and nonlinear theories. In region II, between R_{TC}^{sub} and the overstable critical Rayleigh number R_{TC}^{over}, the fluid remains at rest, according to the linear stability theory (the real part of p is negative), while the nonlinear theory predicts the possible existence of a finite-amplitude convection. Which one of those two modes will prevail depends essentially on the initial conditions used to start the numerical code. In region III, between R_{TC}^{over} and R_{TC}^{osc}, the rest state is unstable and overstability is expected to occur. For this situation, both real and imaginary parts of p are positive and oscillatory flows are possible in this region, the extent of which depends strongly on the values

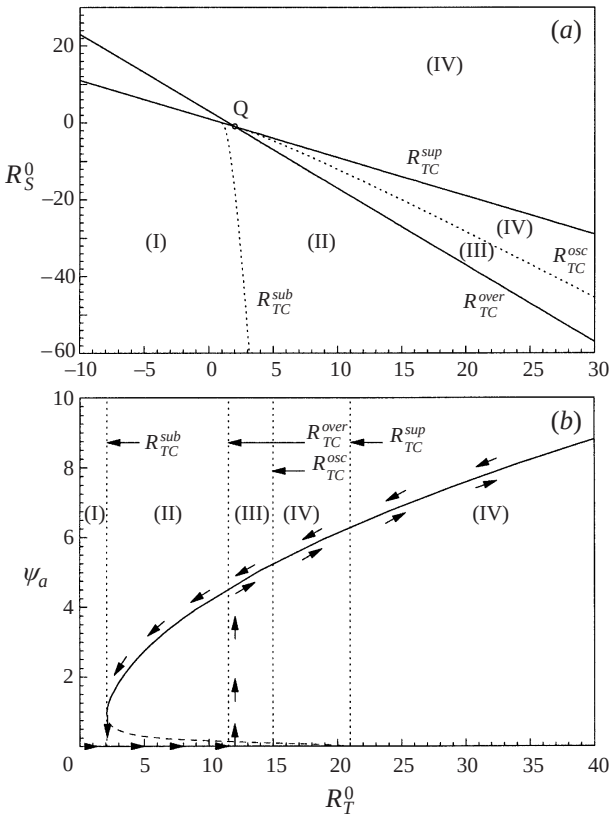

FIGURE 3. (*a*) Stability diagram and (*b*) bifurcation diagram for $R_S^0 = -20$; $Le = 10$ and $\varepsilon = 0.2$.

of Le, A and ε. Above the oscillating critical Rayleigh number, R_{TC}^{osc}, region IV, the fluid is unstable and any infinitesimal perturbation will initiate a direct convective flow. In this region, the real part of p is positive, but the imaginary one is null.

In figure 3(*b*) the normalized stream function amplitude, $\psi_a = \psi_0/\sqrt{a}$, is plotted as a function of the thermal Rayleigh number, R_T^0, for $Le = 10$, $\varepsilon = 0.2$ and $R_S^0 = -20$. The resulting diagram is also independent of the values of A and κ. In the graph the four regions discussed in figure 3(*a*) are indicated for convenience. Upon starting the numerical code with a conductive state or a finite-amplitude convection as initial conditions, when increasing or decreasing R_T^0, the resulting solution may follow the hysteresis loop indicated by arrows. It is observed that below the supercritical value $R_{TC}^{sup} = 21 \times R_0^{sup}$, according to the nonlinear analytical solutions, two convective modes are possible. The solution corresponding to the higher convective mode, represented in the graph by a solid line, was found numerically to be stable. On the other hand, it has not been possible to confirm numerically the existence of the lower convective mode depicted by a dashed line. Since any lower convection motion will grow with time in the range $R_{TC}^{over} \leqslant R_T \leqslant R_{TC}^{osc}$, as predicted by the linear theory, this solution is thus believed to be unstable. According to the linear stability analysis infinitesimal oscillatory motions are induced in the range $R_{TC}^{over} \leqslant R_T \leqslant R_{TC}^{osc}$. However, with this theory nothing can be said about the final state when convection is strong enough such that the nonlinear advection terms overcome the linear ones. As a matter of

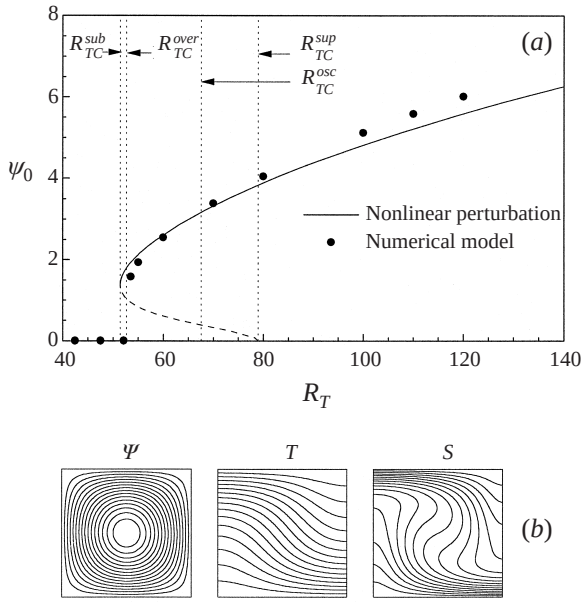

FIGURE 4. (*a*) Bifurcation diagram for $A = 1$, $N = -0.1$, $Le = 5$, $\varepsilon = 1$ and $\kappa = 0$. (*b*) Flow structure and temperature and concentration fields for $R_T = 55$; $\psi_0 = 1.928$, $\overline{Nu} = 1.368$ and $\overline{Sh} = 3.304$.

fact, it was found numerically that, depending on the governing parameters, the final convective flows could be either oscillatory or steady as it will be discussed below.

Figure 4 presents the bifurcation diagram predicted by the nonlinear perturbation theory and the numerical solution for $A = 1$, $N = -0.1$, $Le = 5$, $\varepsilon = 1$ and $\kappa = 0$ (i.e. $R_0^{sup} = 4\pi^2$). For these parameters, the values of the critical Rayleigh numbers are given by $R_{TC}^{sub} = 51.41$, $R_{TC}^{over} = 52.64$, $R_{TC}^{osc} = 67.55$ and $R_{TC}^{sup} = 78.96$. These values are indicated on the graph by dotted vertical lines. In general, the agreement between the nonlinear theory and the numerical results, depicted by solid circles, is good. As expected, this agreement deteriorates as the value of R_T increases due to the severely truncated Fourier series used in the model. The numerical results indicate that, upon decreasing R_T from 120 to 40 step by step using the previous results as initial conditions, a finite-amplitude convective flow can be sustained up to $R_T = 53.3$. Below this value the flow was found to become oscillating and purely conductive for $R_T < 52.64$. On the other hand, when using the rest state as initial conditions and increasing R_T from 40 to 120, it was found that convective flow is possible only for $R_T \geqslant R_{TC}^{over} = 52.64$. Above this value, periodic oscillatory convection is observed for $52.64 < R_T \leqslant 56.7$. Thus, the steady-state branch cannot be reached in this range. In this range, the oscillation time period is observed to increase with R_T. For $56.8 \leqslant R_T < 67.55$, the numerical results demonstrate that the flow starts to oscillate with increasing amplitude and then bifurcates towards a steady convective state predicted by the stable branch.

It is noted that, for the case $\varepsilon = 1$ considered here, the subcritical and the overstable critical Rayeigh numbers, R_{TC}^{sub} and R_{TC}^{over}, are nearly equal. Thus, it is difficult to verify numerically the threshold of the subcritical convection. For this reason, numerical tests have been done for the same governing parameters but with $\varepsilon = 0.2$ for which $R_{TC}^{over} > R_{TC}^{sup}$ (i.e. overstability is not possible). For this situation, it was found possible

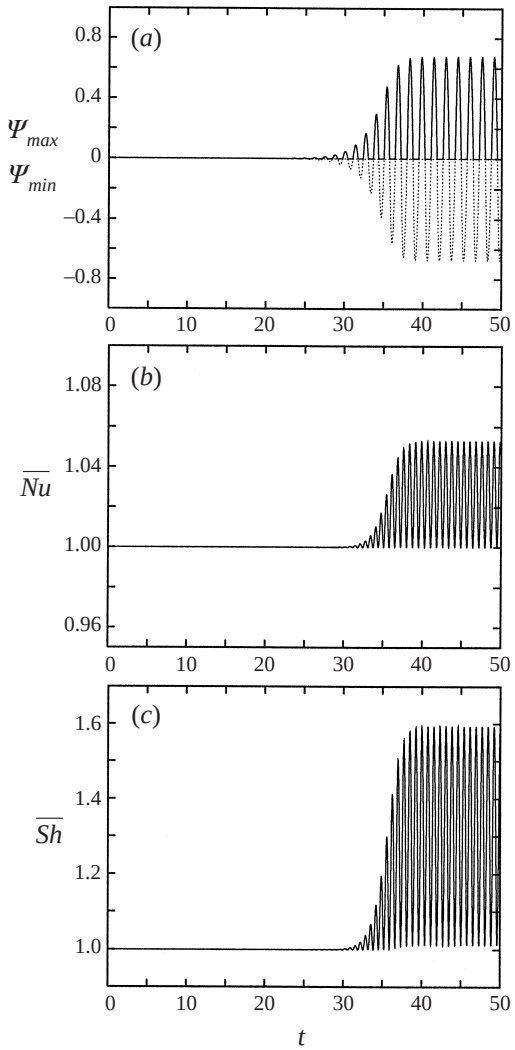

FIGURE 5. Time history, for $R_T = 55$, $N = -0.1$, $Le = 5$, $A = 1$, $\varepsilon = 1$ and $\kappa = 0$, of (a) stream function extrema values ($\Psi_{\min}$ and $\Psi_{\max}$), (b) heat transfer rate ($\overline{Nu}$) and (c) mass transfer rate ($\overline{Sh}$).

to obtain a steady-state convective flows up to $R_T = 53.3$. For $R_T \leqslant 53.2$, the solution was purely diffusive.

In the overstable region, i.e. $52.64 < R_T < 67.55$, the numerical results indicate the existence of two possible convective modes, one steady and the other unsteady. Figure 4(b) illustrates the contour lines of stream function, temperature and concentrations of the steady convective solution obtained for $R_T = 55$, using as initial conditions the steady convective state obtained for a higher Rayleigh number. On the other hand, for the same values of the governing parameters, upon using the rest state as initial conditions ($\psi = 0$, $T = S = -y$) together with a small-amplitude perturbation ($\psi_0 = 10^{-6}$) the resulting convective flow was found to be periodically oscillating. Figures 5(a)–5(c) illustrate the time history of the stream function extrema and the Nusselt and Sherwood numbers, respectively. The results indicate that, as predicted by the linear stability theory, instabilities develop as oscillations of increasing amplitudes.

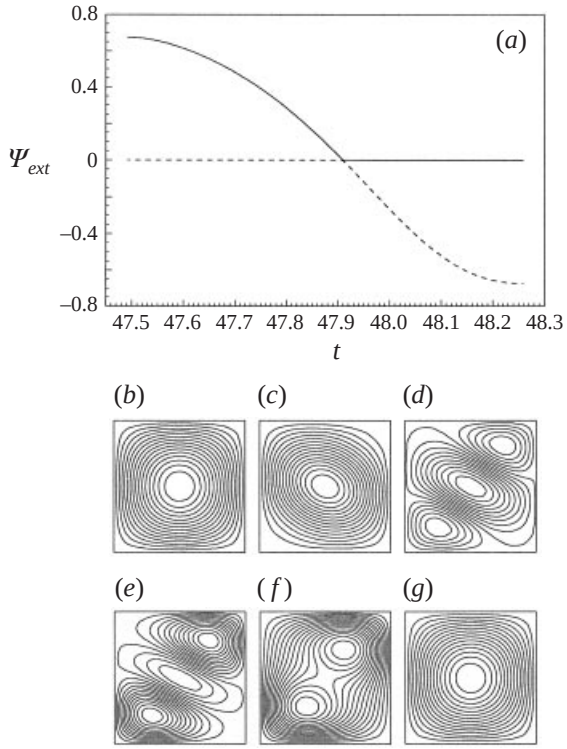

FIGURE 6. (*a*) Time history of the stream function extrema; and selected streamline patterns for (*b*) $t = 47.492$, (*c*) $t = 47.906$, (*d*) $t = 47.9086$, (*e*) $t = 47.909$, (*f*) $t = 47.910$, (*g*) $t = 48.258$; $R_T = 55$, $N = -0.1$, $Le = 5$, $A = 1$, $\varepsilon = 1$ and $\kappa = 0$.

For this situation, the values of the real and imaginary parts of p are $p_r = 0.532$ and $p_i = 4.833$. The period of oscillations ($\tau = 2\pi/p_i$) is thus 1.300. At the beginning of the convective motion ($t \leqslant 20$) it is found numerically that the period of oscillation is $\tau = 1.301 \pm 0.001$, this result being in good agreement with that of the linear stability theory. For $t > 20$ the advection effects become more and more important and eventually the system converges towards a periodic oscillatory regime. For this situation, the period of oscillations has increased to $\tau = 1.535 \pm 0.001$. The numerical results indicate an overturning of the flow from clockwise to counterclockwise circulation and vice versa. Figure 6(*a*) shows the variation of the stream function extrema with time during half a period. At $t = 47.492$, figure 6(*b*) shows that the flow structure consists of a unicellular counterclockwise circulation filling up the entire cavity. Upon increasing t, the strength of the convective flow decreases and the resulting cell is approximately aligned along the diagonal region of the cavity (figure 6*c*). At $t = 47.9086$ two small clockwise rotating eddies are observed to occur at the right top and the left bottom corners, respectively (figure 6*d*). These secondary cells grow in size with time while the primary cell dwindles (figure 6*e*, *f*). At $t = 48.258$, the unicellular clockwise circulation in figure 6(*g*) indicates that a complete reversal of the flow circulation has been achieved. By symmetry (i.e. $\psi(t+\tau/2, x, y) = -\psi(t, -x, y)$), similar flow structure evolution occurs for the remaining half-period. The whole process is repeated during each time period ($\tau = 1.535$).

The above results are concerned only with the case of a square enclosure. Upon keeping the same governing parameters but increasing the aspect ratio up to $A = 5$

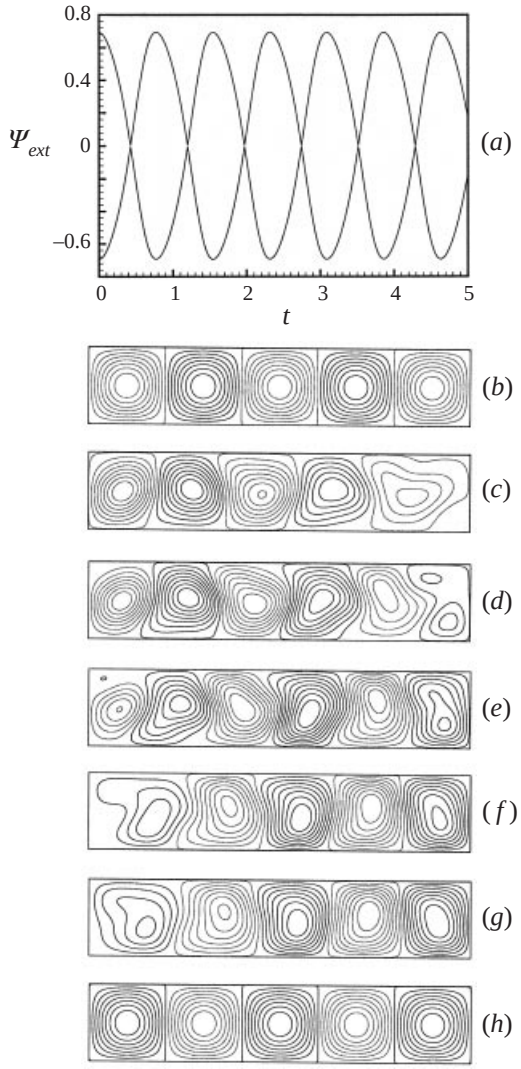

FIGURE 7. (*a*) Time history of the stream function extrema and some selected flow patterns obtained for (*b*) $t = 0.0000$, (*c*) $t = 0.4236$, (*d*) $t = 0.4247$, (*e*) $t = 0.4258$, (*f*) $t = 0.4272$, (*g*) $t = 0.4281$, (*h*) $t = 0.7724$; $R_T = 55$, $N = -0.1$, $Le = 5$, $A = 5$, $\varepsilon = 1$ and $\kappa = 0$.

the resulting steady-state solution (with five cells) was observed to be similar to that reported for $A = 1$. However, the behaviour of the unsteady solution was found to be quite different from that reported in figure 6. Thus, the flow structures, depicted in figure 7 for different times t, show the existence of an oscillating horizontal left-travelling wave with a time period of oscillations of about $\tau = 1.5448$. The cells horizontal motion is observed to occur in a short time period of about 0.005 where ψ_{ext} aproaches zero (see figure 7*a*) and the flow structure becomes asymmetric and consisting of six cells. During this translation period, the cells move to the left by a distance of 1. For an infinite shallow cavity ($A \gg 1$) with Dirichlet boundary conditions, numerical results were obtained for the same governing parameters by considering periodic boundary conditions in the horizontal direction ($f(t, x, y) = f(t, x + A_C, y)$, where f stands for Ψ, T and S and $A_C = 2$ is the critical wavelength)

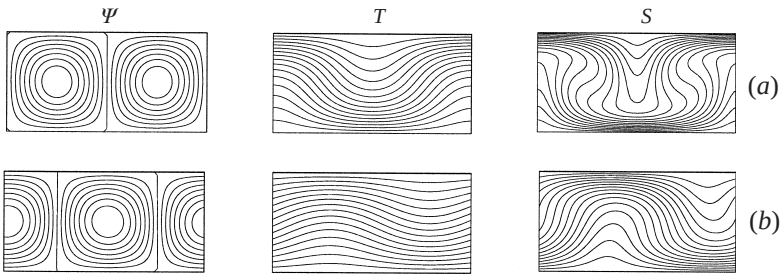

FIGURE 8. Stream lines, isotherms and isoconcentrations in an infinite horizontal layer obtained for $N = -0.1$, $Le = 5$, $\varepsilon = 1$ and $A = A_C = 2$ using periodic boundary conditions in the horizontal direction: (*a*) steady convective state for $R_T = 55$, $\Psi_{\max} = -\Psi_{\min} = 1.924$, $\overline{Nu} = 1.371$, $\overline{Sh} = 3.320$; (*b*) left-travelling wave for $R_T = 53$, $\Psi_{\max} = -\Psi_{\min} = 0.869$, $\overline{Nu} = 1.087$, $\overline{Sh} = 1.865$.

with zero horizontal net flow. For this situation, the values of the four critical Rayleigh numbers, R_{TC}^{sub}, R_{TC}^{over}, R_{TC}^{osc} and R_{TC}^{sup}, are the same as those predicted for a square cavity. Starting the numerical runs with the rest-state solution, it was found that for $R_T = 55$ (in the overstable regime) the solution oscillates at first and then converges towards a steady convective state as depicted in figure 8(*a*). However, for $R_T = 53$ as shown in figure 8(*b*), the final solution is characterized by a left-travelling wave with constant horizontal velocity $u_c = -1.03$. The flow intensity remains constant

4.2. *Parallel flow approximation*

In this section an analytical solution is derived to predict the steady convective regime within a porous enclosure subject to constant fluxes of heat and mass ($\kappa = 1$). With this type of boundary conditions, for small or large aspect ratios A, the problem can be significantly simplified with the help of the parallel flow approximation, as discussed for instance by Mamou *et al.* (1995, 1998*a*). The limiting case of a slender cavity will be considered first.

4.2.1. *Slender cavity* $A \ll 1$

When the aspect ratio A of the cavity is small enough, according to the parallel flow approximation, $u(x, y) \simeq 0$ and $v(x, y) \simeq v(x)$ in the central part of the enclosure. For this situation, it can be demonstrated that the temperature and concentration are linearly stratified in the vertical direction such that $\theta(x, y) = C_\theta\ y + \varphi_\theta(x)$ and $\phi(x, y) = C_\phi\ y + \varphi_\phi(x)$. With these approximations, the governing equations (2.14) can be solved to yield the stream function, temperature and concentration distributions

$$\left.\begin{aligned} \psi(x, y) &= \psi_0 \cos(\omega x), \\ \varphi_\theta(x, y) &= C_\theta\ y - \frac{\psi_0}{\omega} C_\theta \sin(\omega x), \\ \varphi_\phi(x, y) &= C_\phi\ y - \frac{Le\psi_0}{\omega} C_\phi \sin(\omega x), \end{aligned}\right\} \tag{4.38}$$

where ψ_0 is the value of the stream function at the centre of the cavity, C_θ and C_ϕ are the unknown temperature and concentration gradients in the y-direction respectively and

$$\omega = \sqrt{-(R_T\ C_\theta + R_S\ C_\phi)}. \tag{4.39}$$

From the stream function boundary condition, (2.15), it follows that

$$\psi_0 \cos(\omega/2) = 0 \tag{4.40}$$

which indicates that the rest state ($\psi_0 = 0$) is a possible solution which is expected to be stable up to a subcritical Rayleigh number R_{TC}^{sub} (at which a finite-amplitude convective motion bifurcates from the rest state). From (4.40) it is clear that this convective motion implies that

$$\omega = (2n+1)\pi, \qquad n = 0, 1, \ldots . \tag{4.41}$$

In the above relation n corresponds to different flow structures. For $n = 0$, the flow is unicellular and for $n \geqslant 1$ the flow consists of $(2n+1)$ counter-rotating vertical cells.

The balance of heat and solute at each transversal section (at given y) of the enclosure yields

$$C_\theta = -\frac{2/A_y}{2+\psi_0^2}, \qquad C_\phi = -\frac{2/A_y}{2+Le^2\psi_0^2}. \tag{4.42}$$

Upon combining (4.39) and (4.42), it is found that

$$Le^4\psi_0^4 - 2ad_1Le^2\psi_0^2 - a^2d_2 = 0, \tag{4.43}$$

where d_1 and d_2 are similar to those defined in (4.30). For the present situation, $a = 1$ and $R^{sup} = \omega^2 = \pi^2$ for monocellular flows. The solution of (4.43) is similar to that discussed for (4.32).

4.2.2. *Shallow cavity $A \gg 1$*

The case of shallow cavity subject to uniform vertical fluxes of heat and mass has been investigated recently by Mamou *et al.* (1995) on the basis of the parallel flow approximation. Following the procedure described above, the following solution was obtained by these authors:

$$\left.\begin{aligned} \psi &= \psi_0(1-4y^2), \\ \varphi_\theta &= C_\theta x + \frac{C_\theta\psi_0}{3}(3y-4y^3), \\ \varphi_\phi &= C_\phi x + \frac{C_\phi Le\psi_0}{3}(3y-4y^3), \end{aligned}\right\} \tag{4.44}$$

where

$$\psi_0 = \frac{3}{2}\left(R_T^0\ C_\theta + \frac{R_S^0}{Le}\ C_\phi\right). \tag{4.45}$$

The constants C_θ and C_ϕ are given by

$$C_\theta = \frac{4a\ \psi_0}{3(2a+\psi_0^2)}, \qquad C_\phi = \frac{4a\ Le\ \psi_0}{3(2a+Le^2\psi_0^2)}. \tag{4.46}$$

Upon combining the definition of ψ_0, (4.45), and that of C_θ and C_ϕ, (4.46), it is readily found that

$$\psi_0(Le^4\psi_0^4 - 2ad_1Le^2\psi_0^2 - a^2d_2) = 0, \tag{4.47}$$

where d_1 and d_2 are defined in (4.30) with $a = \frac{15}{16}$ and $R^{sup} = 12$. Here again, the solution of (4.47) in terms of ψ_0 is similar to that depicted in (4.31) and (4.32).

4.2.3. *Results and discussion*

Figures 9(*a*) and 9(*b*) illustrate typical bifurcation types, in terms of the flow intensity, $\psi_a = \psi_0/\sqrt{a}$, as a function of R_T^0, R_S^0 (or N) and Le, as predicted by the nonlinear perturbation theory and the parallel flow approximation. With this normalization the curves depicted in the graphs are valid, independently of the values

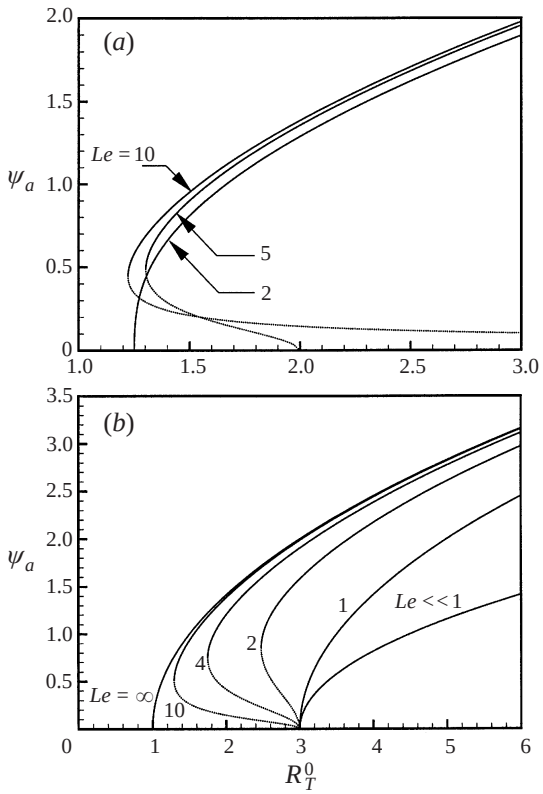

FIGURE 9. Bifurcation diagram as predicted by the parallel flow approximation and the nonlinear theory for (*a*) $N = -0.1$, (*b*) $R_S^0 = -2$.

of A and κ. As mentioned before, the constant a depends solely on A and κ. For instance, $a = 8$ for $\kappa = 0$ and $A = 1$. On the other hand for $\kappa = 1$, $a = \frac{15}{16}$ when $A \gg 1$ and $a = 1$ when $A \ll 1$, respectively.

Figure 9(*a*) exemplifies the effect of the Lewis number on the bifurcation character for $N = -0.1$. For this value, according to (4.37), the Lewis number expressing the transition from a supercritical to a subcritical bifurcation is $Le = 2.154$. As can be observed from the graph, the bifurcation is supercritical when $Le < 2.154$ (i.e. $Le = 2$) and subcritical when $Le > 2.154$ (i.e. $Le = 5$ and 10). Also, as discussed by Mamou (1998) and Mamou, Vasseur & Bilgen (1998*b*), the parameter R^{sup} is infinity when $NLe \leqslant -1$. For this situation, the linear stability analysis indicates that the system is unconditionally stable to small-amplitude perturbation. However, the nonlinear perturbations theory demonstrates the existence of finite-amplitude convection as can be seen from the graph.

Another view of the effect of the Lewis number on the present problem is illustrated in figure 9(*b*) for $R_S^0 = -2$. The Lewis number corresponding to the passage from subcritical to supercritical bifurcation is obtained from (4.36) as $Le = 1.225$. For this reason, all the curves plotted in the graph for $Le > 1.225$ indicate subcritical bifurcation. The limiting curve corresponding to $Le \to \infty$ is also presented in figure 9(*b*) for comparison. For this situation, the solute concentration is almost uniform in the whole cavity, except in very thin layers near the boundaries. For this limit, the critical thermal Rayleigh number for the onset of convection approaches that

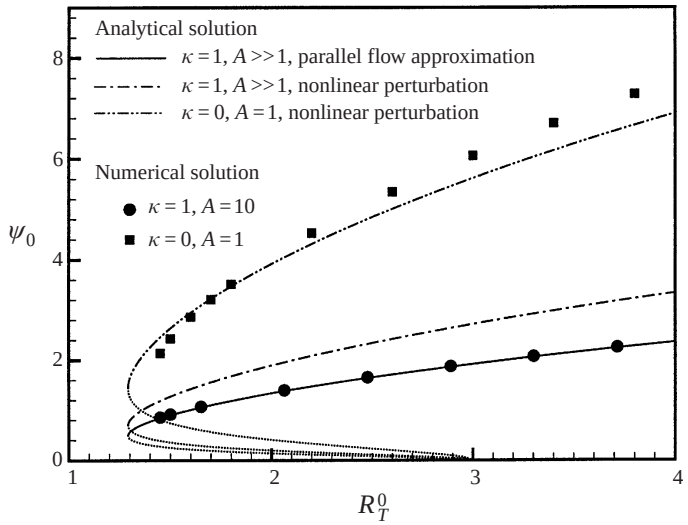

FIGURE 10. Comparison between the nonlinear theory, the parallel flow approximation and the numerical results: bifurcation diagram for $R_S^0 = -2$, $Le = 10$ and $\kappa = 0$ and 1.

corresponding to the onset of Rayleigh–Bénard convection due solely to temperature variations, i.e.

$$R_{TC}^{sub} \to R_0^{sup} \quad \text{and} \quad \psi_0 \to 0 \quad \text{as} \quad Le \to \infty. \tag{4.48}$$

Numerical and nonlinear theory results are presented in figure 10 for $Le = 10$, $R_S^0 = -2$ and $\kappa = 0$ and 1. For this situation, the subcritical Rayleigh number is $R_{TC}^{sub} = 1.291 \times R_0^{sup}$. For a shallow enclosure ($A \gg 1$, $\kappa = 1$ and $R_0^{sup} = 12$), the agreement between the numerical results (obtained for $A = 10$, since, as discussed for instance by Mamou *et al.* 1995, for such a value the flow structure over the central part of the cavity becomes independent of the aspect ratio) and the parallel flow approximation is seen to be excellent. Upon decreasing R_T^0 below 4, the numerical results presented in figure 10 indicate that a steady unicellular flow is possible down to $R_T^0 = 1.45$. In the range $1.3 < R_T^0 < 1.45$ the flow was found to be permanently oscillating. Below $R_T^0 = 1.291$ the numerical results show that convection is not possible. The analytical results, predicted by the nonlinear perturbation theory, for the case $A \gg 1$ and $\kappa = 1$, is depicted in figure 10 by dash-dotted line. It is observed that, due to the severely truncated Fourier series used, the results overestimate the flow intensity. However, it is noted that the subcritical Rayleigh number predicted by this theory is in agreement with the value obtained from the parallel flow approximation.

The case of a square cavity subject to Dirichlet boundary conditions ($A = 1$ and $\kappa = 0$) is also presented in figure 10. Good agreement is observed between the numerical and the nonlinear theory results near the onset of supercritical convection. It is noted that the linear stability analysis predicts that the onset of overstable convection occurs at a critical Rayleigh number R_{TC}^{over} which varies from 1.3 to 3 as the value of ε decreases from 1 to 0.15. For $\varepsilon = 0.15$, $R_{TC}^{over} = R_{TC}^{sup}$ such that, according to the linear stability analysis, subcritical convection is not possible. However, both the nonlinear theory and the numerical results presented in figure 10 indicate that subcritical convection is possible independently of the value of ε and R_{TC}^{over}.

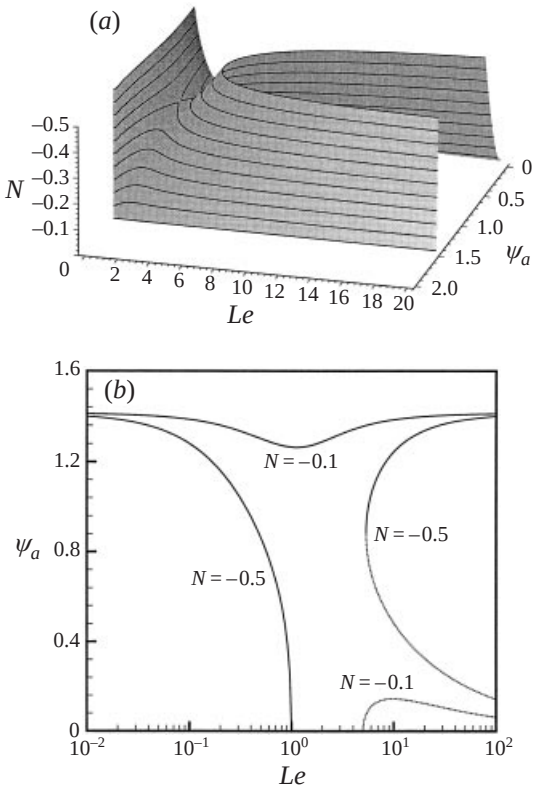

FIGURE 11. Bifurcation diagram as predicted by the parallel flow approximation and the nonlinear theory for $R_T^0 = 2$.

Figure 11 illustrates the effect of the Lewis number, Le, and the buoyancy ratio, N, on the flow intensity, ψ_a, for $R_T^0 = 2$. As can be seen from figure 11(a), the convective flows could be supercritical or subcritical depending on the values of N and Le. For a given value of N, both subcritical and supercritical bifurcations are observed to exist upon varying Le from 0 to 20. Figure 11(b) indicates that for $N = -0.1$, as can be deduced from figure 11(a), the finite-amplitude flow, found for $Le < 2.154$, comes from a subcritical primary bifurcation. The small-amplitude unstable convective branch appears only for $Le > 5$ as it is for this value that the subcritical primary bifurcation point reaches the value $R_T^0 = 2$ chosen in figure 11. For $N = -0.5$, the branch on the left corresponds to flows coming from a supercritical primary bifurcation. This branch disappears at $Le = 1$ when the threshold for this situation becomes larger than the value $R_T^0 = 2$. This bifurcation then becomes subcritical, associated with a saddle-node point (at $Le = 5.36$ such that $R_{TC}^{sub} = R_T = 2 \times R_0^{sup}$) when Le is increased.

Finally, some typical numerical results are presented in figures 12 and 13 for $R_T = 100$, $N = -0.8$, $Le = 10$, $A = 5$, $\varepsilon = 1$ and $\kappa = 1$. These results demonstrate the existence of at least four possible solutions for this set of governing parameters. The first one corresponds to the diffusive regime. Upon starting the numerical code with $\Psi = T = S = 0$ as initial conditions, the rest state was found to remain stable (results are not presented here). The second solution corresponds to a unicellular flow (see figure 12a) for which the flow is parallel in the central part of the cavity,

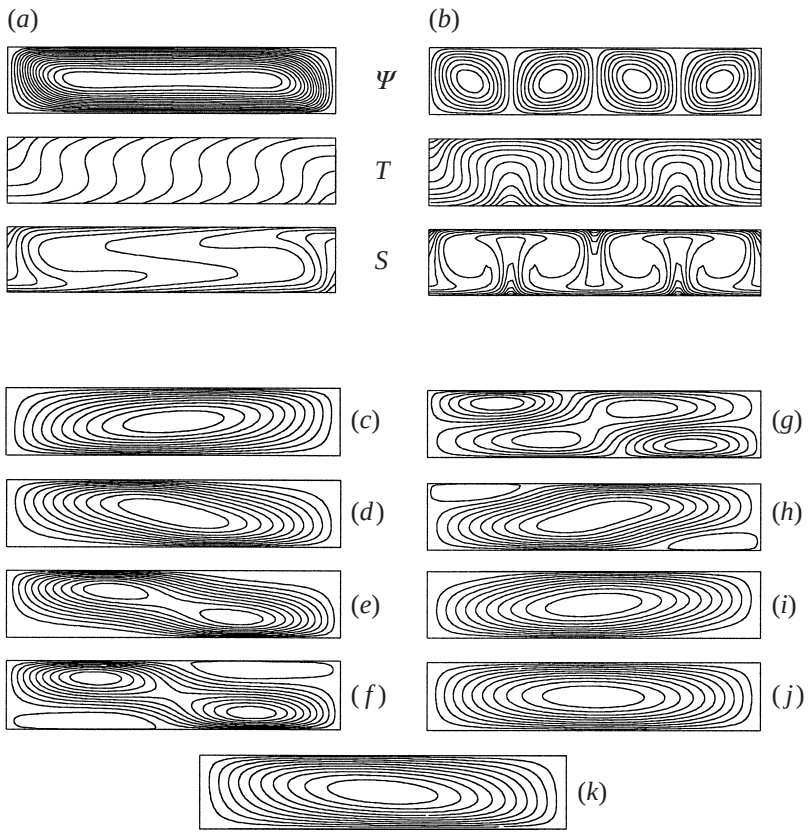

FIGURE 12. Multiple solutions for $R_T = 100$, $N = -0.8$, $Le = 10$, $A = 5$, $\varepsilon = 1$ and $\kappa = 1$; stream function, temperature and concentration patterns are presented for three different possible solutions in (*a*) monocellular flow, (*b*) Bénard flow and (*c–k*) unsteady flow. (*a*) $\Psi_{max} = 3.689$, $\Psi_{min} = 0$, $\overline{Nu} = 3.635$ and $\overline{Sh} = 6.739$, (*b*) $\Psi_{max} = 3.412$, $\Psi_{min} = -3.412$, $\overline{Nu} = 2.459$ and $\overline{Sh} = 8.288$, (*c*) $t = 5.150$, (*d*) $t = 6.741$, (*e*) $t = 7.000$, (*f*) $t = 7.093$, (*g*) $t = 7.187$, (*h*) $t = 7.276$, (*i*) $t = 7.364$, (*j*) $t = 7.535$ and (*k*) $t = 8.692$.

in agreement with the analytical predictions. This solution was obtained by using, as initial conditions, a unicellular flow calculated previously for another set of governing parameters. Also, using a multi-cellular flow pattern as initial conditions yielded the Bénard flow structure depicted in figure 12(*b*) (third solution). Recently, convection in a shallow porous layer heated from below by a constant flux was studied by Kimura *et al.* (1995). The transient development of the velocity and temperature fields from the rest state was investigated by these authors. The formation of a number of cells, whose horizontal dimensions had roughly the same order of magnitude as the height of the cavity, was initially observed. These convective cells gradually merged together to form horizontal elongated cells, and eventually a single cell. The time taken to reach a steady state was found to be relatively high and to depend on the aspect ratio of the cavity. For this reason, the computations presented in figure 12(*b*) were carried out up to a dimensionless time as high as approximately 500 in order to ensure that a steady state has been reached. Finally, a unicellular flow with a small amplitude was also tried as initial conditions for the present problem. It was found that the resulting solution evolves towards a permanently oscillating state of convection in which the flow circulation changes from a clockwise to counterclockwise direction and

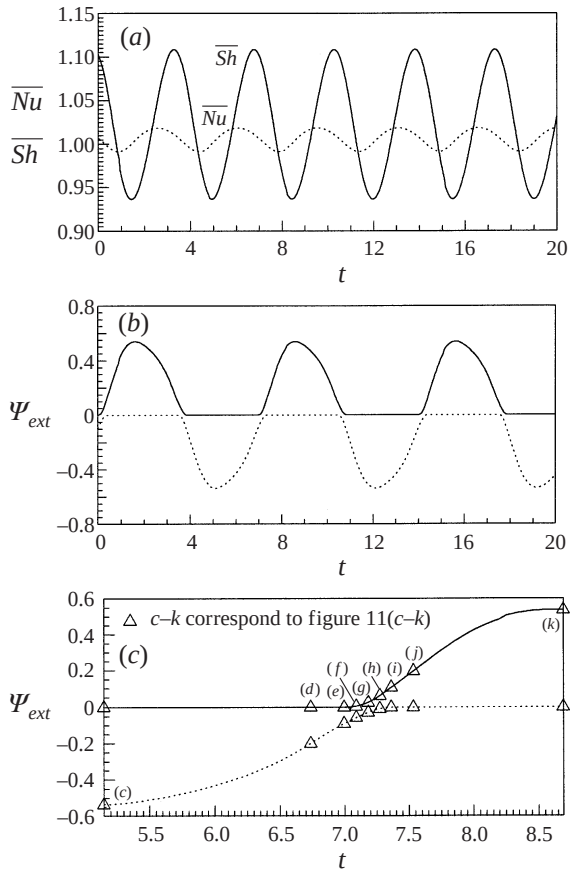

FIGURE 13. Nusselt and Sherwood numbers and stream function extrema versus time for opposing flows for $R_T = 100$, $N = -0.8$, $Le = 10$, $A = 5$, $\varepsilon = 1$ and $\kappa = 1$.

vice versa (fourth solution, see figure 12*c–k*). The time evolution of the corresponding stream function extrema and Nusselt and Sherwood numbers are shown in figure 13. A physical explanation for the existence of such oscillating flows, for double-diffusive convection, has been given by many authors (see, for instance, Rosenberg & Spera 1992).

5. Conclusion

The onset and development of double-diffusive convection in a rectangular cell subject to vertical gradients of heat and solute have been investigated analytically and numerically. Results are obtained for different types of thermal and solutal boundary conditions, namely Dirichlet and Neumann types. The stability of the system was studied analytically using both linear and nonlinear perturbation theories. When the layer is subject to uniform fluxes of heat and solute, analytical solutions have been derived, for the limiting case of shallow or slender layers, on the basis of the parallel flow approximation. Also, a numerical solution of the full governing equations was obtained using the finite element method.

The main conclusions of the present analysis are as follows.

(i) Instabilities via stationary or oscillatory modes have been determined analyt-

ically, on the basis of the linear and nonlinear perturbation theories, in terms of the governing parameters of the problem. Four different regimes are found to exist, namely the pure diffusive regime, the subcritical convective regime, the overstable regime and the supercritical regime. Domains of existence of the different regimes were found to depend on the solutal to thermal buoyancy ratio, the Lewis number, the aspect ratio of the cavity, the normalized porosity of the porous medium and the thermal and solutal boundary condition type.

(ii) For finite-amplitude flows, in the vicinity of the onset of supercritical convection, two types of bifurcation are predicted by the nonlinear analytical models proposed in the present study. For the first one, called subcritical bifurcation, the convective flow bifurcates from the rest state through finite-amplitude convection. This type of bifurcation occurs only for the case of opposing buoyancy forces and when the Lewis number is greater than unity. The threshold characterized by the subcritical Rayleigh number was found to be a function of the buoyancy ratio, the Lewis number, the aspect ratio of the enclosure and the thermal and solutal boundary condition types. For the second one, called supercritical bifurcation, the convective flow bifurcates from the rest state with zero amplitude. This type of bifurcation exists for additive flows and for opposing flows with a Lewis number smaller than unity. Despite the severely truncated Fourier series used in the nonlinear perturbation analysis, the agreement between the analytical and the numerical results, in the neighbourhood of the onset of supercritical convection, is acceptable. On the other hand, the parallel flow approximation was found to be in agreement with the numerical results, independently of the strength of the convective motion, provided that the aspect ratio of the cavity is made large (or small) enough.

(iii) The existence of multiple solutions, for a given set of the governing parameters, is demonstrated numerically for the case of opposing flows. Thus, depending upon the initial conditions used to start the numerical code, a pure diffusive state, unicellular and multicellular steady flows and permanently oscillating flows could be observed in the system. For an infinite horizontal layer, a steady convective state and horizontal travelling wave are observed.

REFERENCES

Ahlers, G. & Lücke, M. 1987 Some properties of an eight-mode Lorenz model for convection in binary fluids. *Phys. Rev.* A **35**, 470–473.

Bergman, T. L. & Shrinivasan, R. 1989 Numerical simulation of Soret-induced double diffusion in an initially uniform concentration binary fluid. *Intl J. Heat Mass Transfer* **32**, 679–687.

Brand, H. & Steinberg, V. 1983 Nonlinear effects in the convective instability of a binary mixture in a porous medium near threshold. *Phys. Lett.* **93A**, 333–336.

Chen, F. & Chen, C. F. 1993 Double-diffusive fingering convection in a porous medium. *Intl J. Heat Mass Transfer* **36**, 793–807.

Cheng, P. 1978 Heat transfer in geothermal systems. *Adv. Heat Transfer* **44**, 1–105.

De Groot, S. R. & Mazur, P. 1962 *Non Equilibrium Thermodynamics*. North Holland.

Horton, C. W. & Rogers, F. T. 1945 Convection currents in a porous medium. *J. Appl. Phys.* **16**, 367–370.

Kimura, S., Vynnycky, M. & Alavyoon, F. 1995 Unicellular natural circulation in a shallow horizontal porous layer heated from below by a constant flux. *J. Fluid Mech.* **294**, 231–257.

Lapwood, E. R. 1948 Convection of a fluid in a porous medium. *Proc. Camb. Phil. Soc.* **44**, 508–521.

Malashetty, M. S. 1993 Anisotropic thermoconvective effects on the onset of double diffusive convection in a porous medium. *Intl J. Heat Mass Transfer* **36**, 2397–2401.

Mamou, M. 1998 Convection thermosolutale dans des milieux poreux et fluides confinés. PhD thesis, Ecole Polytechnique de Montréal, Québec, Canada.

Mamou, M., Vasseur, P. & Bilgen, E. 1998*a* Double diffusive convection instability problem in a vertical porous enclosure. *J. Fluid Mech.* **368**, 263–289.

Mamou, M., Vasseur, P. & Bilgen, E. 1998*b* A Galerkin finite-element study of the onset of double-diffusive convection in an inclined porous enclosure. *Intl J. Heat Mass Transfer* **41**, 1513–1529.

Mamou, M., Vasseur, P., Bilgen, E. & Gobin, D. 1995 Double-diffusive convection in an inclined slot filled with porous medium. *Eur. J. Mech.* B/*Fluids* **14**, 629–652.

Murray, B. T. & Chen, C. F. 1989 Double-diffusive convection in a porous medium. *J. Fluid Mech.* **201**, 147–166.

Nield, D. A. 1968 Onset of thermohaline convection in porous medium. *Water Resour. Res.* **4**, 553–560.

Nield, D. A. & Bejan, A. 1999 *Convection in Porous media.* Springer.

Platten, J. K. & Legros, J. C. 1984 *Convection in Liquids.* Springer.

Poulikakos, D. 1986 Double diffusive convection in a horizontal sparcely packed porous layer. *Intl Commun. Heat Mass Transfer* **13**, 587–598.

Rosenberg, N. D. & Spera, F. J. 1992 Thermohaline convection in a porous medium heated from below. *Intl J. Heat Mass Transfer* **35**, 1261–1273.

Rudraiah, N., Shrimani, P. K. & Friedrich, R. 1982 Finite amplitude convection in a two-component fluid saturated porous layer. *Intl J. Heat Mass Transfer* **25**, 715–722.

Taunton, J. W. & Lightfoot, E. N. 1972 Thermohaline instability and salt fingers in a porous medium. *Phys. Fluids* **15**, 748–753.

Trevisan, O. V. & Bejan, A. 1987 Mass and heat transfer by high Rayleigh number convection in a porous medium heated from below. *Intl J. Heat Mass Transfer* **30**, 2341–2356.

Vasseur, P., Satish, M. G. & Robillard, L. 1987 Natural convection in a thin, inclined, porous layer exposed to a constant heat flux. *Intl J. Heat Mass Transfer* **30**, 537–549.

Veronis, G. 1968 Effect of a stabilizing gradient of solute on thermal convection. *J. Fluid Mech.* **34**, 315–336.